

Connecting Direct Dark Matter Detection Experiments to Cosmologically Motivated Halo Models

Yao-Yuan Mao, Louis E. Strigari, Risa H. Wechsler

Kavli Institute for Particle Astrophysics and Cosmology & Physics Department, Stanford University, Stanford, CA 94305; SLAC National Accelerator Laboratory, Menlo Park, CA, 94025

Several direct detection experiments, including very recently CDMS-II, have reported signals consistent with 5 to 10 GeV dark matter that appear to be in tension with null results from XENON experiments. We establish the cosmologically motivated parameter space for the Galactic dark matter velocity distribution function (VDF) and illustrate that seemingly contradictory experimental results with the standard analysis can be made consistent with each other within this VDF parameter space. Future experimental limits should be reported for a range of well-motivated VDFs.

PACS numbers: 95.35.+d, 98.35.Gi

Introduction. — Dark matter comprises roughly 80% of the matter in the universe and seeds the formation of galaxies and large-scale structure. Weakly Interacting Massive Particles (WIMPs) are well-motivated candidates for dark matter, and many theoretical WIMP candidates have been proposed [1–4]. Though WIMPs have not been detected, a variety of direct, indirect, and collider experiments are rapidly progressing in their searches for them [5].

Despite rapidly improving sensitivities and analysis methods, several direct detection experiments are presenting a conflicting picture. The DAMA [6], COGENT [7], and CRESST [8] collaborations have reported hints for low mass dark matter in the mass range $\sim 5 - 10$ GeV. Most recently, the CDMS-II collaboration has reported three events in their silicon detectors that are not explained by known backgrounds, which when interpreted as a WIMP signal yields a most likely mass of 8.6 GeV [9]. However, all these candidate events are inconsistent with the null result reported by the XENON100 collaboration [10]. Proposed ideas to alleviate the conflict include improved characterization of experimental backgrounds [11, 12], particle physics explanations such as tuning the ratio of the coupling constants of WIMP scattering on neutrons and protons [13], or more detailed examination of the local dark matter density and the velocity distribution function (VDF) [14–16].

The so-called “Standard Halo Model” (SHM), which specifies the VDF to be a Maxwell–Boltzmann distribution with a cutoff at the escape velocity, is commonly adopted by direct detection experiments. As a consequence, uncertainties in the VDF are not a standard component of the analysis of experimental data. For heavy WIMPs, greater than ~ 20 GeV, it is relatively safe to neglect the uncertainties in the VDF because the majority of modern experiments are not sensitive to the variation of the VDF in this high-mass regime. However, for lighter WIMPs, which have been a large focus of recent experimental efforts, uncertainties the VDF may significantly

affect experimental results.

Several recent studies have shown that the Maxwell–Boltzmann velocity distribution is not well-motivated from the perspective of cosmological simulations in a Lambda Cold Dark Matter (LCDM) universe [17, 18], and different VDF models have been proposed that better describe simulated halos [14, 16]. Methods to present and to compare results from different experiments without assuming a specific VDF model have been developed [15, 19–21], though a VDF model is still required to translate results from individual experiments into constraints or limits on physical parameters of the dark matter particle [22–26].

It has not yet become a standard in the direct detection community to include the uncertainties of the VDF or to use a VDF-independent presentation in their published results, possibly because the traditional vanilla WIMP candidate has mass of ~ 100 GeV and in this regime the experiments are less subject to impact of the VDF. As intriguing signals continue to mount, and new theoretical models of low mass dark matter are constructed [13, 27–29], it is important to systematically address the issue of the VDF in the context of direct detection experiments and establish well-motivated models for it. In a recent analysis of cosmological simulations, Mao *et al.* [16, hereafter Paper I] have empirically determined that the VDF in dark matter halos may be described by the following functional form with two parameters (v_0, p) ,

$$f(|\mathbf{v}|) = \begin{cases} A \exp(-|\mathbf{v}|/v_0) \left(v_{\text{esc}}^2 - |\mathbf{v}|^2 \right)^p, & 0 \leq |\mathbf{v}| \leq v_{\text{esc}} \\ 0, & \text{otherwise.} \end{cases} \quad (1)$$

Paper I showed that a family of VDFs in the form of Eq. 1 are consistent with current cosmological simulations, and also that (v_0, p) depends primarily on the quantity r/r_s , the radial position where the VDF is measured, normalized by the scale radius of the density profile of the halo. Due to the unknown scale radius of the Milky Way dark matter halo, the halo-to-halo scatter in (v_0, p) from simulations, the scatter at a fixed position within a given

halo, and the potential impact of baryonic physics, there still exist significant uncertainties in the VDF, and hence in direct detection event rates.

In this paper we explicitly identify the range of the parameter space described by Eq. 1 that is allowed by cosmological simulations. We further demonstrate that, within this well-motivated parameter domain, there is large range of predicted event rates for a WIMP model with a fiducial mass of 8.6 GeV, and show that it is possible to simultaneously explain the CDMS-II, CoGENT, and XENON100 results by simply by changing from the SHM to a more cosmologically motivated VDF. This opens up the intriguing possibility that the tension between these experiments is resolved by uncertainties in the Milky Way halo model, and motivates the development of a stronger connection between cosmological simulations and predicted direct detection event rates. We conclude by discussing the current sources of the uncertainties in the VDF, the possibilities for eliminating the uncertainties, and suggest how to mitigate these uncertainties in the experiment analysis.

The Distribution of the VDF Parameters. — We first identify a domain of allowed parameter space from cosmological simulations of dark matter halos for the VDF of Eq. (1). Paper I identifies the best-fit VDF parameters v_0/v_{esc} and p of individual halos from simulations, and indicates an apparent correlation between these two parameters for a fixed r/r_s . This degeneracy between v_0/v_{esc} and p impedes a simple description of the parameter domain of interest. To break this degeneracy, we instead find it useful to parameterize the VDF of Eq. (1) by $v_{\text{rms}}/v_{\text{esc}}$ and p , where v_{rms} is the root-mean-square velocity, defined as

$$v_{\text{rms}} \equiv \left[4\pi \int_0^{v_{\text{esc}}} dv v^4 f(v) \right]^{1/2}. \quad (2)$$

For notational simplicity, hereafter we use v_{rms} and v_0 to refer to their respective normalized values, $v_{\text{rms}}/v_{\text{esc}}$ and v_0/v_{esc} .

In Figure 1 we show the value of v_{rms} as a function of (v_0, p) . There is an one-to-one correspondence between (v_{rms}, p) and (v_0, p) , so the VDF of Eq. (1) can be completely specified by (v_{rms}, p) . Furthermore, lines of constant v_{rms} follow the relation between v_0 and p for a fixed r/r_s ; v_{rms} is largely determined by r/r_s , while the halo-to-halo scatter is primarily determined by the parameter p . This is physically explained by noting that v_{rms} is the ratio of the average energy to the escape energy, which is directly related to the relative position in the gravitational potential.

With this parameterization, we can now specify the parameter domain of interest within cosmological simulations. Figure 2 shows the 90% scatter on the VDF parameters for three different samples of simulated halos. One sample is from the RHAPSODY simulation [30], in which

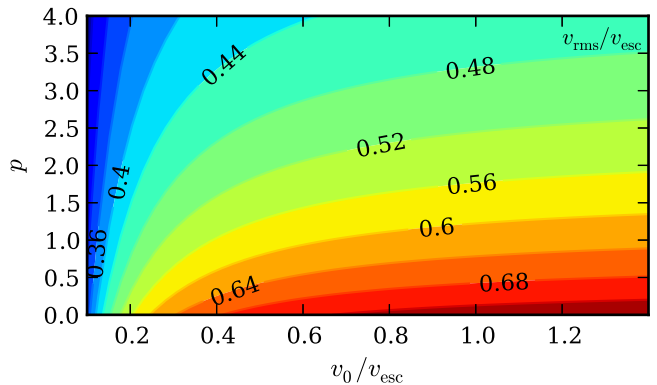


FIG. 1. Contours show the value of $v_{\text{rms}}/v_{\text{esc}}$ as a function of $(v_0/v_{\text{esc}}, p)$, from the VDF model of Eq. 1.

there are 96 halos with virial mass of $\sim 10^{14.8} M_{\odot} h^{-1}$. The other two samples are halos with virial mass of $\sim 10^{14} M_{\odot} h^{-1}$ and of $\sim 10^{13} M_{\odot} h^{-1}$ respectively, in the the BOLSHOI simulation [31]. We use samples of halos with different masses in order to determine if there are mass trends of the VDF parameters. As shown in Paper I and more explicitly in Figure 2, there is no mass trend indicated over three orders-of-magnitude in mass, implying that it is reasonable to apply the following analysis to Milky Way mass halos.

We set the domain of interest on v_{rms} based on the current observational constraint on r/r_s , which is, conservatively, $[0.15, 1.2]$ [16, and references therein]. This then sets the domain of interest on v_{rms} to be $[0.35, 0.52]$. Since the parameter p is not affected by r/r_s , guided by the 90% halo-to-halo scatter from Figure 2 we set the domain of interest on p to be $[0, 3]$. We note that the magnitude of the halo-to-halo scatter is comparable to the directional scatter at a fixed radius within an individual halo, so the above domain will not shrink even if one could remove the halo-to-halo scatter completely, given our lack of knowledge about the Earth's angular position. These constraints may be modified by future observational results or a better understanding of the dark matter distribution in simulated halos; we discuss if there are foreseeable improvements of the constraints on this domain of interest in the last section. For the sole purpose of demonstrating the impact of the VDF on the direct detection, one could take this full domain of interest to be the allowed VDF parameter space given modern numerical simulations.

A Demonstration with Mock Experiments. — We demonstrate the impact of uncertainties in the VDF on direct detection experiments by considering two mock experiments, which we call Exp. X and Exp. S, and investigate how the different parameters of the VDF in Eq. 1 impact the interpretation of the results. In this demonstration, we assume a WIMP model which has a mass $m_{\text{dm}} = 8.6$ GeV and a WIMP-nucleon cross section at

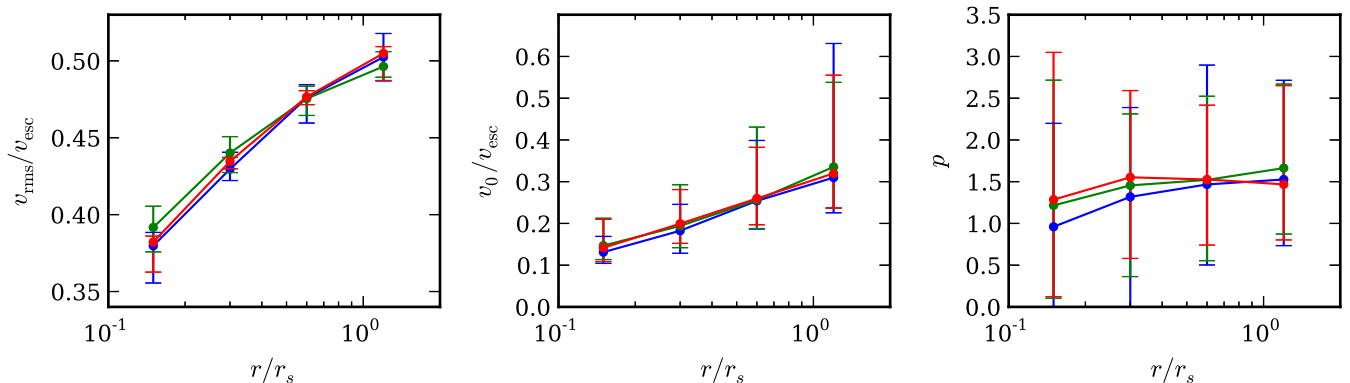


FIG. 2. From left to right, the plots show $v_{\text{rms}}/v_{\text{esc}}$ (from fitted profiles), fitted v_0 , and fitted p respectively, as functions of r/r_s , for simulated dark matter halos of three samples. The red sample consists of halos of $\sim 10^{13} M_{\odot}$ in the BOLSHOI simulation, the green sample consists of halos of $\sim 10^{14} M_{\odot}$ in the BOLSHOI simulation, and the blue sample consists of all halos in the RHAPSODY simulation ($\sim 10^{14.7} M_{\odot}$). The errorbars show the 90% halo-to-halo scatter of each sample.

zero momentum transfer $\sigma_0 = 1.9 \times 10^{-41} \text{ cm}^2$, as inspired by the recent results from the CDMS-II experiment [9]. Note that this mass and cross section are also consistent with the recent CoGENT analysis [32].

For Exp. X we consider Xenon as the target nucleus, with a nuclear recoil energy threshold of 6 keV, and an exposure of 6000 kg-days. For Exp. S we consider Silicon as the target nucleus, with a recoil energy threshold of 7 keV, and an effective exposure of 7.1 kg-day, chosen to obtain a mean event count of 3 in the case of the SHM. In both experiments, to highlight the theoretical impact of the VDF we assume a sharp energy cutoff at the threshold energy, and both perfect energy response efficiency and energy resolution. We fix the local dark matter density to be $\rho_0 = 0.3 \text{ GeV/cm}^3$, and assume equal WIMP coupling to the neutron and proton. We set the Galactic escape velocity to be 544 km/s, and take average speed of the Earth in the Galactic frame to be 232 km/s.

Given the parameters stated above, we can then calculate the predicted event rate R , which is the integral of the differential event rate per unit detector mass over the recoil energy Q ,

$$R = \int_{Q_{\text{thres}}} \frac{dR}{dQ} dQ, \quad (3)$$

and

$$\left. \frac{dR}{dQ} \right|_Q = \frac{\rho_0 \sigma_0}{2\mu^2 m_{\text{dm}}} A^2 |F(Q)|^2 \int_{v_{\text{min}}(Q)} d^3v \frac{f(\mathbf{v} + \mathbf{v}_e)}{v}. \quad (4)$$

Here μ is the WIMP-nucleon reduced mass, A is the atomic number of the nucleus, $|F(Q)|^2$ is the nuclear form factor [33], $v_{\text{min}} = (Qm_N/2\mu^2)^{1/2}$ for an elastic collision, f is the VDF in the Galactic rest frame, and \mathbf{v}_e is the velocity of Earth in the Galactic rest frame.

The question we address in this demonstration is how

the probability of a certain experiment observing N collision events (assuming all the events are real WIMP-nucleus collisions) varies with different models for the VDF. We define P_X to be the probability that Exp. X observes *no* events, and P_S the probability that Exp. S observes three events. We calculate the probabilities assuming that WIMP-nucleon collision events follow a Poisson process,

$$P(N|\lambda) = \frac{\lambda^N}{N!} e^{-\lambda}, \quad (5)$$

where N is the number of events, which equals 0 for P_X and 3 for P_S , and λ is a dimensionless parameter that equals the predicted rate times the exposure of the experiment. Note that λ changes with the WIMP model, the experimental setup, and the VDF. In the demonstration we always fix the WIMP model and the settings of each of the two experiments, and only change the VDF to see its effect.

Assuming the SHM, we obtain $P_X = 4.65 \times 10^{-7}$ and $P_S = 0.224$. With these assumptions (including the sharp energy cutoff), given the low P_X , Exp. X rejects the WIMP model at a high confidence level. So if Exp. S does indeed observe WIMP events, it implies a strong tension between these two experiments. Note that when the SHM is assumed, this conflict remains for any escape velocity larger than 515 km/s. However, the results change dramatically if a different VDF model is assumed. Assuming the VDF in Eq. (1) with a range of parameters motivated from cosmological simulations, we calculate P_X and P_S and show the results in Figure 3.

The uncertainties in the VDF can have distinct effects on the different experiments. Figure 3 shows that P_X is a strong function of p , while P_S only mildly depends on v_{rms} and is insensitive to p . Because different experiments have different responses to changes in the VDF, a given VDF can reconcile two experiments that are in-

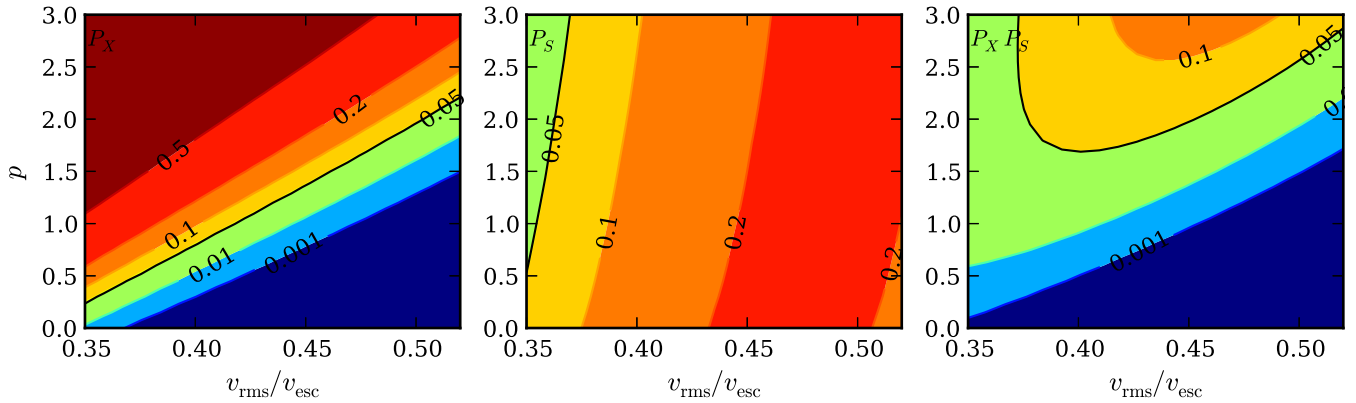


FIG. 3. The contours show the probabilities P_X (left), P_S (middle), and $P_X \times P_S$ (right), as functions of the VDF parameters $v_{\text{rms}}/v_{\text{esc}}$ and p in the region of interests. Color scales on the three plots are all the same. P_X is the probability that Exp. X observes *no* event, and P_S is the probability that Exp. S observes 3 events. Values below 0.05 are excluded with 95 percent confidence. High values of p can significantly reduce the tension between the two experiments, when compared to the SHM. See text for details of the mock experiments and other assumptions.

consistent with one another when using the SHM.

In the left panel of Figure 3, we see that Exp. X, which is strongly ruled out with the Standard Halo Model VDF, can only reject less than half of the parameter domain at a 95% confidence level when the VDF is allowed to vary. On the other hand, Exp. S could still observe three events, given that $P_S > 0.05$ for almost all v_{rms} and p within the ranges shown on Figure 3. In the right most panel we also show the joint probability $P_X \times P_S$. In roughly one-third of the parameter domain, the possibility of Exp. S observing three events and Exp. X observing none cannot be excluded. In order to exclude this WIMP model for all possible VDF considered within this domain, we find that Exp. X must lower its energy threshold to at least 5.25 keV, if all other conditions and assumptions unchanged. This may be possible with forthcoming xenon-based experiments [34].

As a reminder, the above analysis does not include the effect of background noise, the energy cutoff, the energy response efficiency, and the energy resolution of the mock experiments, and hence caution should be invoked when drawing strong conclusions about the relationship between XENON100 and CDMS-II experiments. However, it does clearly motivate a full self-consistent statistical analysis with a VDF of the form Eq. (1) because if the dark matter is in fact a light WIMP, a model for the VDF will be required to translate measurements into physical parameters of the dark matter particle.

Quantifying Uncertainty from the VDF. — The results of the above demonstration can be also interpreted as follows: under the assumption of the WIMP model, if Exp. S observes three true WIMP events and the Exp. X observes none, the SHM is ruled out by the experiments, while some range of our VDF parameter space is still allowed. Within this allowed VDF parameter space, from the perspective of cosmological simulations is there a sin-

gle preferred set of the VDF parameters that could be adopted by experimentalists? Unfortunately, there is a range of uncertainties that impede a simple choice.

Paper I presented a detailed discussion of the sources of scatter. Here we further distinguish these sources according to their contribution to the uncertainties in v_{rms} or in p . We find here that v_{rms} is largely determined by r/r_s ; the uncertainty in this parameter is thus driven by observational uncertainty in r/r_s for the position of the solar system with respect to the density profile of the Milky Way. Conservative estimates of the concentration parameter of the Milky Way imply the region of v_{rms} used in Figure 3; with more optimistic assumptions one can constrain $r/r_s \in [0.32, 0.50]$ [35]. This will narrow the parameter range shown in Figure 3 but would not change our conclusions. It is likely that future data on the motions of Milky Way halo stars and satellites will be able to further constrain the density profile of our Galaxy's halo to minimize this uncertainty. We note that the present analysis considers only dark matter simulations; further study should confirm whether the relationship between v_{rms} and r/r_s is impacted by baryonic physics.

The uncertainty in p , on the other hand, at present appears to be irreducible. The halo-to-halo scatter in p could originate from the different intrinsic properties between halos, but we have not yet found any significant correlations between p and physical properties of the halo (even if found, the quantity may not be well-constrained observationally). In principle, one could ignore the halo-to-halo scatter if we had a simulation that resembles the Milky Way halo in every way; however, there would still be intra-halo scatter due to variation of VDF in various angular positions at a fixed radius. In Paper I, we found that the intra-halo directional scatter is not smaller than the halo-to-halo scatter. Last but not least, baryons could also possibly impact the shape of the VDF as char-

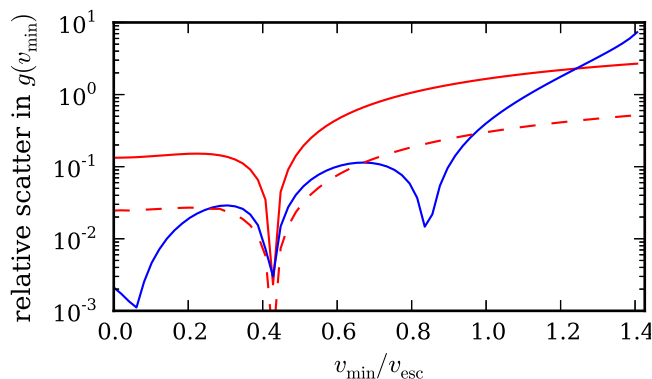


FIG. 4. The relative scatter in $g(v_{\min})$, as defined in text, as a function of v_{\min}/v_{esc} . The red solid line shows the effect of $v_{\text{rms}} \in [0.35, 0.52]$ (while fixing $p = 1.5$), the red dashed line shows the effect of a reduced parameter space $v_{\text{rms}} \in [0.43, 0.46]$ (while fixing $p = 1.5$), and the blue solid line shows the effect of $p \in [0, 3]$ (while fixing $v_{\text{rms}} = 0.45$).

acterized by p .

Given that there is not a single *preferred* set of the VDF parameters, when making statistical statements about signals or exclusions, one should marginalize over the VDF parameters. For example, one can calculate the scatter due to VDF in the differential rate, which is proportional to the quantity

$$g(v_{\min}) \equiv \int_{v_{\min}} d^3v \frac{f(\mathbf{v} + \mathbf{v}_e)}{v} \quad (6)$$

$$= \frac{2\pi}{v_e} \int_{\max(v_{\min}-v_e, 0)}^{v_{\text{esc}}} dy y L(y) f(y), \quad (7)$$

where

$$L(y) = \min(y + v_e - v_{\min}, 2y, 2v_e) \quad (8)$$

and other variables are all defined in the same way as in Eq. (4). For the VDF of Eq. (1) and the parameter domain of interest we introduced previously, we calculate the relative scatter of $g(v_{\min})$ for different v_{\min} . Here we define relative scatter to be the range (the difference between the maximum and the minimum) of a set of values divided by the mean of the same set. The relative scatter of $g(v_{\min})$ due to the uncertainty in v_{rms} and p are shown separately on Figure 4. At larger v_{\min} (higher energy bins), the scatter of $g(v_{\min})$ mainly comes from the uncertainty in p , and at lower v_{\min} , from the uncertainty in v_{rms} , but the latter may be minimized to be comparable to the uncertainty in p if r/r_s can be better determined. We note that features on the plot are due to the non-zero speed of the Earth in the Galactic frame. Since this plot shows the *scatter* of $g(v_{\min})$ between halos or regions within the halo, these features do not show up on the energy spectra of the detection experiments.

In conclusion, we show that when one assumes a single parameterized model for the VDF, results from different

experiments cannot be directly compared. Even when restricting to cosmologically motivated VDFs that we have discussed, there is a wide range of interpretations possible for current experimental results. Consequently, to present experimental results we believe the best strategy is to either use a VDF-independent method [15, 19, 21], which most conservatively only compares the region of v_{\min} that is explicitly probed by the experiments, or to use more different VDFs (for example, the SHM, the model of Eq. (1) with $(v_0, p) = (0.2, 3)$, and that with $(v_0, p) = (0.215, 1.5)$) to highlight the possible uncertainties. When making statistical statements about signals or exclusions, one should marginalize over the VDF parameters; here we provide the cosmologically relevant domain of interest over which to do this.

This work was supported by the U.S. Department of Energy under contract number DE-AC02-76SF00515 and by a KIPAC Enterprise Grant. YYM is supported by a Weiland Family Stanford Graduate Fellowship. We thank Blas Cabrera and Peter Sorensen for useful discussions. We also thank Hao-Yi Wu and Oliver Hahn for providing access to the RHAPSODY simulations, Anatoly Klypin and Joel Primack for providing access to the BOLSHOI simulations, and Peter Behroozi for the halo catalogs for both simulations. Our work used computational resources at SLAC.

-
- [1] G. Jungman, M. Kamionkowski, and K. Griest, *Phys. Rept.* **267**, 195 (1996).
 - [2] G. Bertone, D. Hooper, and J. Silk, *Phys. Rept.* **405**, 279 (2005).
 - [3] G. Bertone, *Particle Dark Matter : Observations, Models and Searches* (Cambridge University Press, 2010).
 - [4] J. L. Feng, *Ann. Rev. Astron. Astrophys.* **48**, 495 (2010).
 - [5] L. E. Strigari, (2012), [arXiv:1211.7090 \[astro-ph.CO\]](#).
 - [6] R. Bernabei *et al.* (DAMA Collaboration, LIBRA Collaboration), *Eur. Phys. J.* **C67**, 39 (2010).
 - [7] C. E. Aalseth *et al.* (CoGeNT collaboration), *Phys. Rev. Lett.* **106**, 131301 (2011).
 - [8] G. Angloher, M. Bauer, I. Bavykina, A. Bento, C. Bucci, *et al.*, *Eur. Phys. J.* **C72**, 1971 (2012).
 - [9] R. Agnese *et al.* (CDMS Collaboration), [arXiv:1304.4279 \[hep-ex\]](#).
 - [10] E. Aprile *et al.* (XENON100 Collaboration), *Phys. Rev. Lett.* **109**, 181301 (2012).
 - [11] J. Collar and N. Fields, (2012), [arXiv:1204.3559 \[astro-ph.CO\]](#).
 - [12] P. Sorensen, *Phys. Rev.* **D86**, 101301 (2012).
 - [13] J. L. Feng, J. Kumar, D. Marfatia, and D. Sanford, *Phys. Lett.* **B703**, 124 (2011).
 - [14] M. Lisanti, L. E. Strigari, J. G. Wacker, and R. H. Wechsler, *Phys. Rev.* **D83**, 023519 (2011).
 - [15] M. T. Frandsen, F. Kahlhoefer, C. McCabe, S. Sarkar, and K. Schmidt-Hoberg, *JCAP* **1201**, 024 (2012).
 - [16] Y.-Y. Mao, L. E. Strigari, R. H. Wechsler, H.-Y. Wu, and O. Hahn, *Astrophys. J.* **764**, 35 (2013).
 - [17] M. Vogelsberger, A. Helmi, V. Springel,

- S. D. White, J. Wang, *et al.*, *Mon. Not. Roy. Astron. Soc.* **395**, 797 (2009).
- [18] M. Kuhlen, N. Weiner, J. Diemand, P. Madau, B. Moore, *et al.*, *JCAP* **1002**, 030 (2010).
- [19] P. J. Fox, J. Liu, and N. Weiner, *Phys. Rev.* **D83**, 103514 (2011).
- [20] P. Gondolo and G. B. Gelmini, *JCAP* **1212**, 015 (2012).
- [21] M. T. Frandsen, F. Kahlhoefer, C. McCabe, S. Sarkar, and K. Schmidt-Hoberg, (2013), [arXiv:1304.6066 \[hep-ph\]](#).
- [22] L. E. Strigari and R. Trotta, *JCAP* **0911**, 019 (2009).
- [23] A. H. Peter, *Phys. Rev.* **D81**, 087301 (2010).
- [24] M. Pato, L. Baudis, G. Bertone, R. Ruiz de Austri, L. E. Strigari, *et al.*, *Phys. Rev.* **D83**, 083505 (2011).
- [25] M. Pato, L. E. Strigari, R. Trotta, and G. Bertone, *JCAP* **1302**, 041 (2013).
- [26] B. J. Kavanagh and A. M. Green, (2013), [arXiv:1303.6868 \[astro-ph.CO\]](#).
- [27] J. L. Feng, J. Kumar, and L. E. Strigari, *Phys. Lett.* **B670**, 37 (2008).
- [28] D. E. Kaplan, M. A. Luty, and K. M. Zurek, *Phys. Rev.* **D79**, 115016 (2009).
- [29] R. Essig, J. Mardon, and T. Volansky, *Phys. Rev.* **D85**, 076007 (2012).
- [30] H.-Y. Wu, O. Hahn, R. H. Wechsler, Y.-Y. Mao, and P. S. Behroozi, *Astrophys. J.* **763**, 70 (2013).
- [31] A. A. Klypin, S. Trujillo-Gomez, and J. Primack, *Astrophys. J.* **740**, 102 (2011).
- [32] C. Kelso, D. Hooper, and M. R. Buckley, *Phys. Rev.* **D85**, 043515 (2012).
- [33] J. Lewin and P. Smith, *Astropart. Phys.* **6**, 87 (1996).
- [34] D. Akerib *et al.* (LUX Collaboration), *Nucl. Instrum. Meth.* **A704**, 111 (2013).
- [35] P. R. Kafle, S. Sharma, G. F. Lewis, and J. Bland-Hawthorn, *Astrophys. J.* **761**, 98 (2012).